Journal of Nuclear Materials 396 (2010) 189–196

Contents lists available at ScienceDirect

Journal of Nuclear Materials

journal homepage: www.elsevier.com/locate/jnucmat

Effect of magnesium on the lead induced corrosion and SCC of alloy 800 in neutral crevice solution at high temperature

A. Palani [a], B.T. Lu [a], L.P. Tian [a], J.L. Luo [a,*], Y.C. Lu [b]

[a] Department of Chemical and Materials Engineering, University of Alberta, Edmonton, Alberta, Canada T6G 2G6
[b] Component Life Technology, Stn. 80, Atomic Energy of Canada Ltd. Chalk River Laboratories, Chalk River, Ontario, Canada K0J 1J0

ARTICLE INFO

Article history:
Received 16 May 2009
Accepted 3 November 2009

Keywords:
SCC
Lead
Alloy 800
High temperature
Corrosion
Magnesium

ABSTRACT

Dissolved magnesium species in the feed water reduce the incidence of lead-induced stress corrosion cracking (PbSCC) of Alloy 800. The passivity of material was improved by replacing a part of chlorides in the lead-contaminated chemistry with magnesium chloride, as indicated by: (1) a higher pitting potential; (2) lower passive current densities; (3) a film structure with less defects and more spinel oxides. According to the constant extension rate tensile (CERT) tests conducted in the neutral crevice solutions at 300 °C, lead contamination would reduce the ultimate tensile strength (UTS) and elongation of material. The CERT test results were in agreement with the fracture morphology observations. Magnesium addition significantly reduced the detrimental effect of lead contamination.

1. Introduction

The economic viability of nuclear power infrastructure depends on the safe and reliable operation of pressurized water reactors (PWRs) to minimize any unexpected shutdown. Failure of steam generator (SG) tubes on the secondary side is the major concern in nuclear power plants. These SG tubes are subject to stress corrosion cracking (SCC) in heat transfer crevices associated with tube supports, where the harmful species may be highly concentrated. SCC may develop when the local concentration of harmful species exceeds certain threshold levels [1–3]. Lead contamination found in sludge has been recognized as a primary contributor to SCC [2–7]. Laboratory studies showed that lead contamination as low as 0.01 ppm can induce SCC [2,3].

Alloy 600 has been used for manufacture of SG tubes since the 1960s. Because of the high SCC susceptibility of Alloy 600 in lead-contaminated environments, more resistant materials, such as Alloys 800 and 690, have been used [8]. Alloy 800 is currently widely used as SG tubing material in CANDU[1] systems [9]. The evaluation of SCC susceptibility under plausible CANDU service conditions is practically important for establishing the strategy of water management and the life prediction for the SG tubing.

It has been recognized that the development of SCC in the SG tubing alloys is related to the passive film breakdown. Lead impurities in solution can be incorporated into the passive film and increase the likelihood of breakdown [10,11]. Experimental evidence showed a relationship between the rupture ductility of a passive film and SCC susceptibility of Alloy 800 [12]. In addition to Pb, other species like Cu, Al, Mg, etc. are also present in the sludge, hence there are complex local chemistries [7]. Limited data suggest that both passivity and SCC susceptibility are affected by these species [2,3,9,11]. However, the interactive effects of lead with theses species and their role in lead induced SCC (PbSCC) are still poorly understood. In this study, the effect of magnesium on the passivity and SCC susceptibility of Alloy 800 has been determined for lead contaminated neutral crevice solutions at 300 °C.

2. Experimental procedure

2.1. Materials and solutions

The tubing material is a commercial Fe–Ni based alloy, UNS N08800, and its composition is given in Table 1. Samples were cut from a thick wall pipe. The specimens for electrochemical measurements had a surface area of 2 cm^2 with a spot welded with nickel–chrome wire (80% Cr and 20% Ni) for electric connection. Heat shrinkable Teflon tubing was used to seal the nickel chromium wire and the electric connection. The tensile specimens had a gauge length of 25.4 mm and a gauge diameter of 3.14 mm. Each specimen was ground with silicon carbide paper of grit size 600 and the grinding direction was always parallel to the applied load to reduce the effect of stress concentration at

* Corresponding author. Tel.: +1 780 492 2232; fax: +1 780 492 2881.
E-mail address: jingli.luo@ualberta.ca (J.L. Luo).

[1] CANDU is registered trade mark of Atomic Energy Canada Ltd.

0022-3115/$ - see front matter © 2009 Elsevier B.V. All rights reserved.
doi:10.1016/j.jnucmat.2009.11.004

Table 1
Composition of UNS N08800 (wt.%).

Al	C	Cr	Mn	S	Si	Ti	Cu	Ni	Fe
0.210	0.013	20.300	0.700	<0.0005	0.610	0.530	0.096	32.340	44.800

Table 2
Composition of test solutions.

ID	NaCl (M)	KCl (M)	$CaCl_2$ (M)	Na_2SO_4 (M)	$MgCl_2$ (M)	PbO (mM)	NaOH (M)	pH at 300 °C
N1	0.3	0.05	0.15	0.15	–	–	–	6.1
N2	0.3	0.05	0.15	0.15	–	2.2	–	6.88
N3	0.15	0.05	0.15	0.15	0.075	2.2	0.1445	6.1
N4	–	0.05	0.15	0.15	0.15	2.2	0.2945	6.1

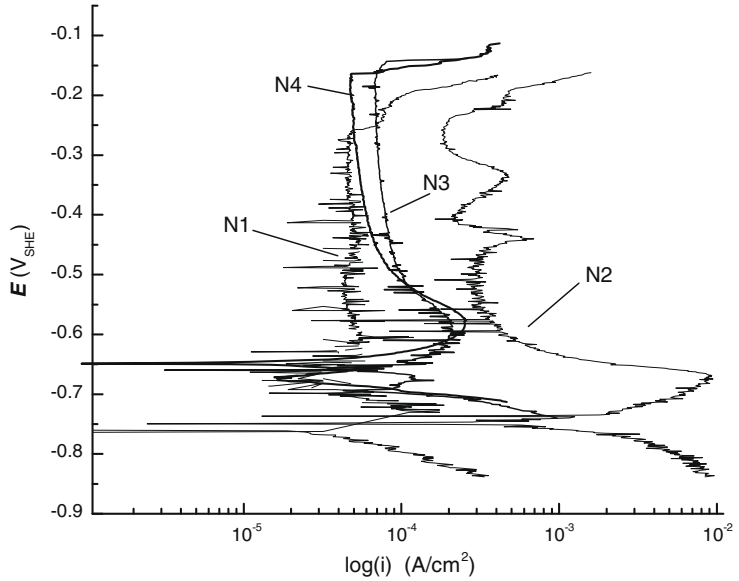

Fig. 1. Polarization diagram of UNS N08800 at 300 °C in neutral crevice solution.

the scratches created by grinding on the crack initiation. Then each specimen was cleaned sequentially with distilled water and acetone.

The solutions used for the investigation are listed in Table 2 and were designed carefully to simulate the actual crevice conditions that prevail in CANDU SG tubes. Solution N1 is the standard neutral crevice solution and N2 is made by the addition of lead oxide to N1 solution. To study the effect of magnesium, 0.075 M $MgCl_2$ or 0.15 M $MgCl_2$ was added to replace a part of standard metal chlorides in the lead-contamination chemistry without changing the total chloride concentration and pH. The solution ion concentrations were calculated using commercial software (OLI).

2.2. Electrochemical measurements

Electrochemical measurements were conducted in an autoclave with a three-electrode electrochemical system at 300 °C. The counter electrode was a platinum wire welded to a platinum mesh and the reference electrode was an Ag/AgCl/KCl electrode [13]. Before the autoclave was heated up, the solution was purged with high purity nitrogen to create an anaerobic condition. All the potentials were converted to standard hydrogen electrode unless otherwise stated. A Camry 3.2 electrochemical measurement system was used in the electrochemical experiments.

Mott–Schottky measurements were performed with a CMS 300 EIS to determine the electronic properties of the passive film. The potential was scanned in the anodic direction in the passive range at 5 mV per step and an AC signal with a frequency of 1000 Hz, and peak-to-peak magnitude of 10 mV was superimposed on the scanning potential. AC impedances were measured as a function of potential. The capacitance values were calculated from the imaginary part of impedance, assuming an equivalent circuit with resistance–capacitance in series because the impedance of the capacitance of the space charge layer is much smaller than that of the charge transfer resistance of the passive film at 1000 Hz [14].

2.3. Surface analyses

The specimens were passivated at the open circuit potential (OCP) for 24 h at 300 °C before each surface analysis. X-ray photoelectron spectroscopy (XPS) measurements were performed using an Axis-ULTRA (Kratos Analytical) spectrometer controlled by a SUN workstation. Photoelectron emission was excited by an aluminium (monochromatized) source operated at 210 W with initial photon energy 1486.71 eV. The survey spectra were recorded at steps of 0.33 eV using 160 eV pass energy, whereas high-resolution spectra were taken at steps of 0.1 eV using 20 eV pass energy. The base pressure was approximately 5×10^{-10} Torr. The C1s peak from adventitious carbon at 284.6 eV was used as a reference to

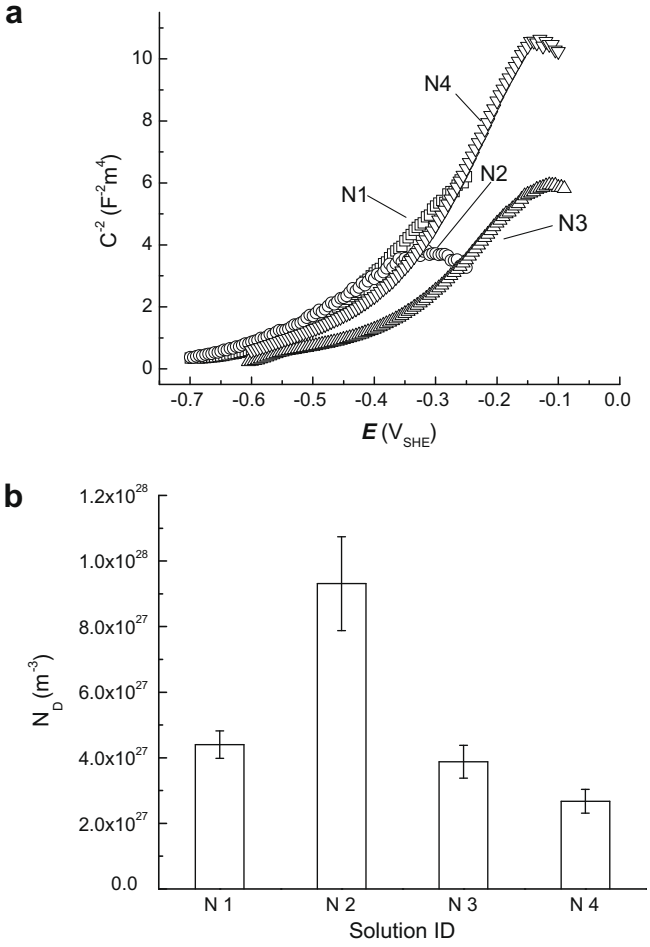

Fig. 2. Mott–Schottky plots: (a) and donor densities and (b) in the passive films.

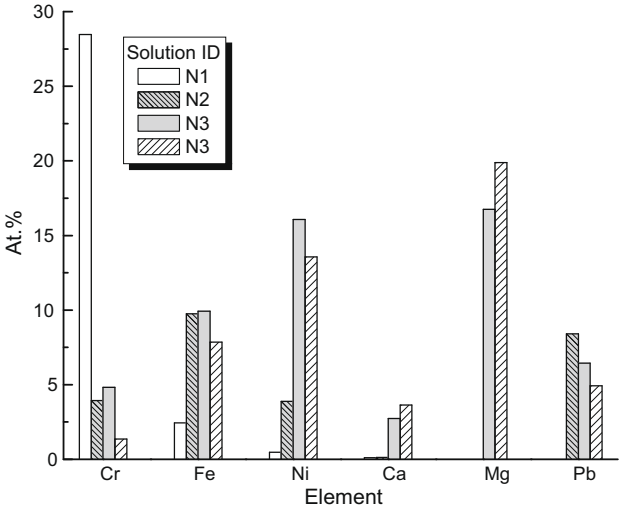

Fig. 4. Effects of solution chemistry on passive film composition.

correct the charging shifts. The photoelectrons were collected at a take-off angle of 90° with respect to the sample surface. Depth profiling was performed over an area of $1.5 \times 1.5\ mm^2$ under 3 keV Ar-ion sputtering; the sputter rate was estimated to be 0.5 nm/min based upon calibration using a silica specimen. The measurements started after 120 s of sputtering to minimize the interference of surface contaminations.

Grazing incidence X-ray diffraction analysis (GIXRD) was carried out using a Rigaku rotating anode RU-200B system equipped with a cobalt anode as X-ray source (40 kV, 160 mA). A thin film setup (vs. wide angle) was used in the measurement. The incident angle was 1°.

2.4. Constant extension rate tensile (CERT) test

Experiments were conducted at 300 °C in an autoclave. The solution was purged with high purity nitrogen before the experiment and anaerobic conditions were maintained throughout the experiment. Once the temperature reached 300 °C the experiment started with the constant extension rate of 1.322×10^{-4} mm/s

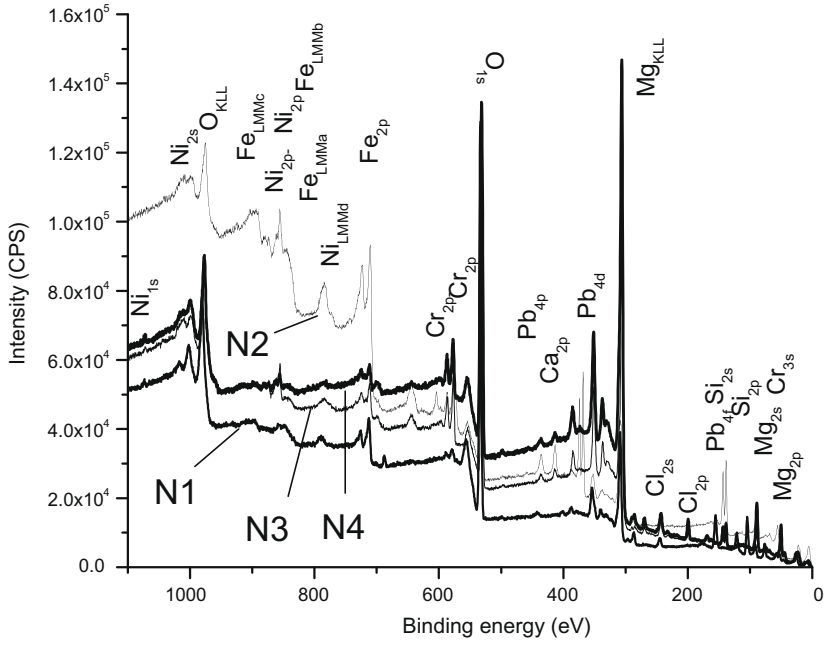

Fig. 3. XPS survey spectra.

until the tensile specimen broke. Then the specimen was taken from the autoclave, cleaned with acetone and prepared for SEM examination.

3. Results and discussion

3.1. Polarization behavior

Polarization behavior of Alloy 800 in neutral crevice chemistry is shown in Fig. 1. As observed in the previous studies [15,10,16], the presence of lead contamination gives rise to an active current peak appearing at the potential around −0.7 V_{SHE} and a higher passive current density. The addition of magnesium chloride into the lead-contaminated chemistry reduced the detrimental effects of lead contamination, as indicated by a smaller active current peak and a lower passive current density. The inhibiting effect of magnesium species in lead-contaminated solution was also demonstrated by a higher pitting potential. An increase in the concentration of magnesium species (N3 vs. N4) reduced the passive current density slightly.

3.2. Mott–Schottky analysis

Mott–Schottky plots in Fig. 2a shows that the passive films of test materials were essentially an n-type semiconductor. It is well known that the defect concentration in an n-type semiconductor can be assessed by its donor density, and is inversely proportional to the slope of a Mott–Schottky plot (Eq. (1)),

$$k_{MS} = \frac{2}{\varepsilon\varepsilon_0 e N_D} \quad (1)$$

where ε is the dielectric constant of the passive film, ε_0 is the permittivity of vacuum, e is the electric charge of an electron and ND is the donor density. As indicated by the Mott–Schottky plots in Fig. 4a, the changes in the chemical compositions of solutions altered the slopes of the plots. The dielectric constants of the oxides of main alloy elements, namely, Fe, Ni and Cr, were in range 11.9–14.2 while that of PbO was 25.9 [17]. Since the maximum atomic percentage of lead incorporated into the passive film was 1.68 at.%, the change in dielectric constant of passive film due to lead incorporation was expected to be limited [11]. Hence the changes in slope of the Mott–Schottky plots were caused mainly by the increment in donor density. A higher donor density implies a more defective passive film structure [18]. Taking $\varepsilon = 15.6$ [19], the donor densities of passive films that were obtained from Mott–Schottky plots in Fig. 2a are given in Fig. 2b. It can be seen that the incorporation of lead impurities increased the donor density in the passive film. On the other hand, magnesium addition reduced the detrimental effect of lead contamination on the passive film structure, as indicated by a reduced donor density. This effect was enhanced with increasing concentration of magnesium species in the test solution.

During the process of passive film formation, cation vacancies were created at the film–electrolyte interface and anion vacancies were created in the metal–film interface. According to the point defect model (PDM) developed by Macdonald [20], the cation vacancies produced at the film/electrolyte interface move towards the metal/film interface and oxygen vacancies move the other way. If the Pb^{2+} ion entering the passive film occupies the divalent cation vacancy, such as V''_{Ni} or V''_{Fe}, this kind of reaction will result in the annihilation of a Schottky defect pair in the passive film. If a lead ion occupies a trivalent cation vacancy, such as, V'''_{Cr} or V'''_{Fe} in the passive film, one-half of oxygen vacancies would be created to maintain the electric neutrality. The later reaction will give rise to an increase in the donor concentration. However, the concentration of lead in passive film is rather low. It is not sufficient to cause the changes in donor density with the amplitude shown in Fig. 2b. Such a change in donor density was more likely to be related to certain changes in passive film structure [11,21].

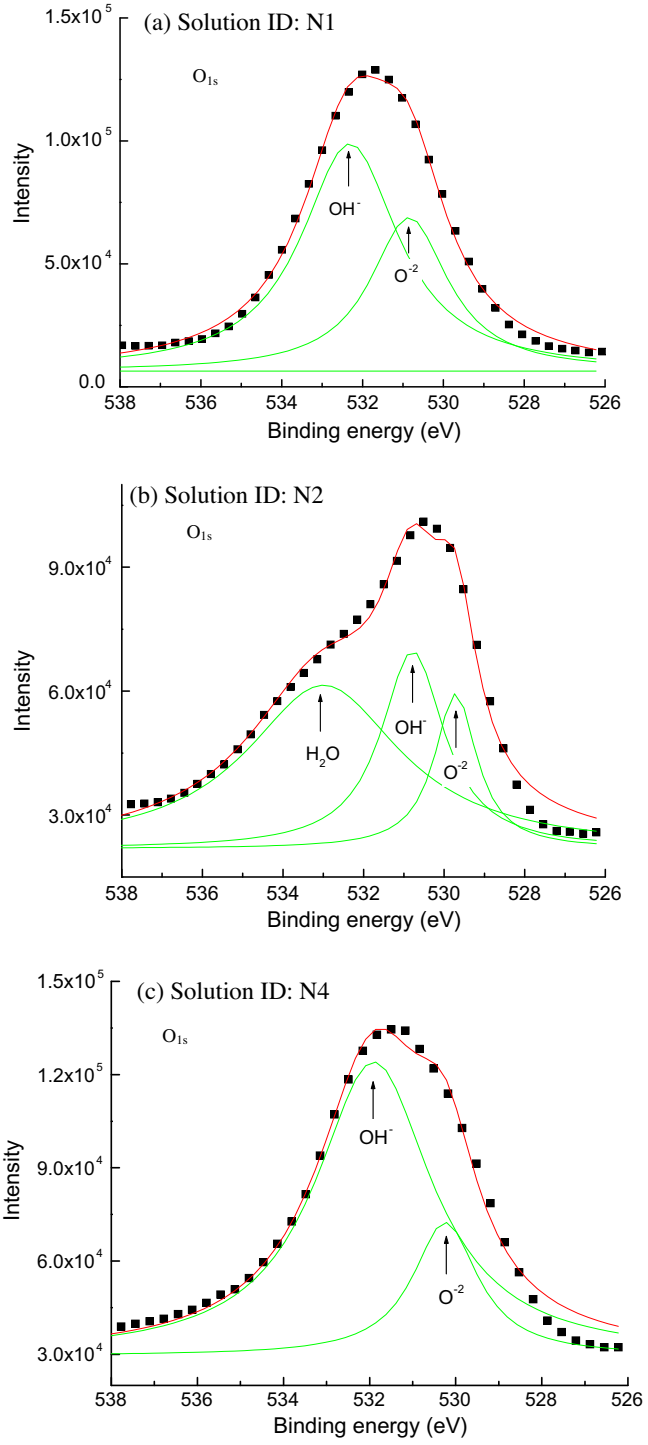

Fig. 5. O1s peaks determined from XPS: (a) solution ID: N1; (b) solution ID: N2; (c) solution ID: N4.

3.3. XPS analysis

It has been recognized that the dissolved lead in a solution can enter the passive film [6,11,10,22,23]. This also was demonstrated in the XPS of Alloy 800 passivated in the neutral crevice

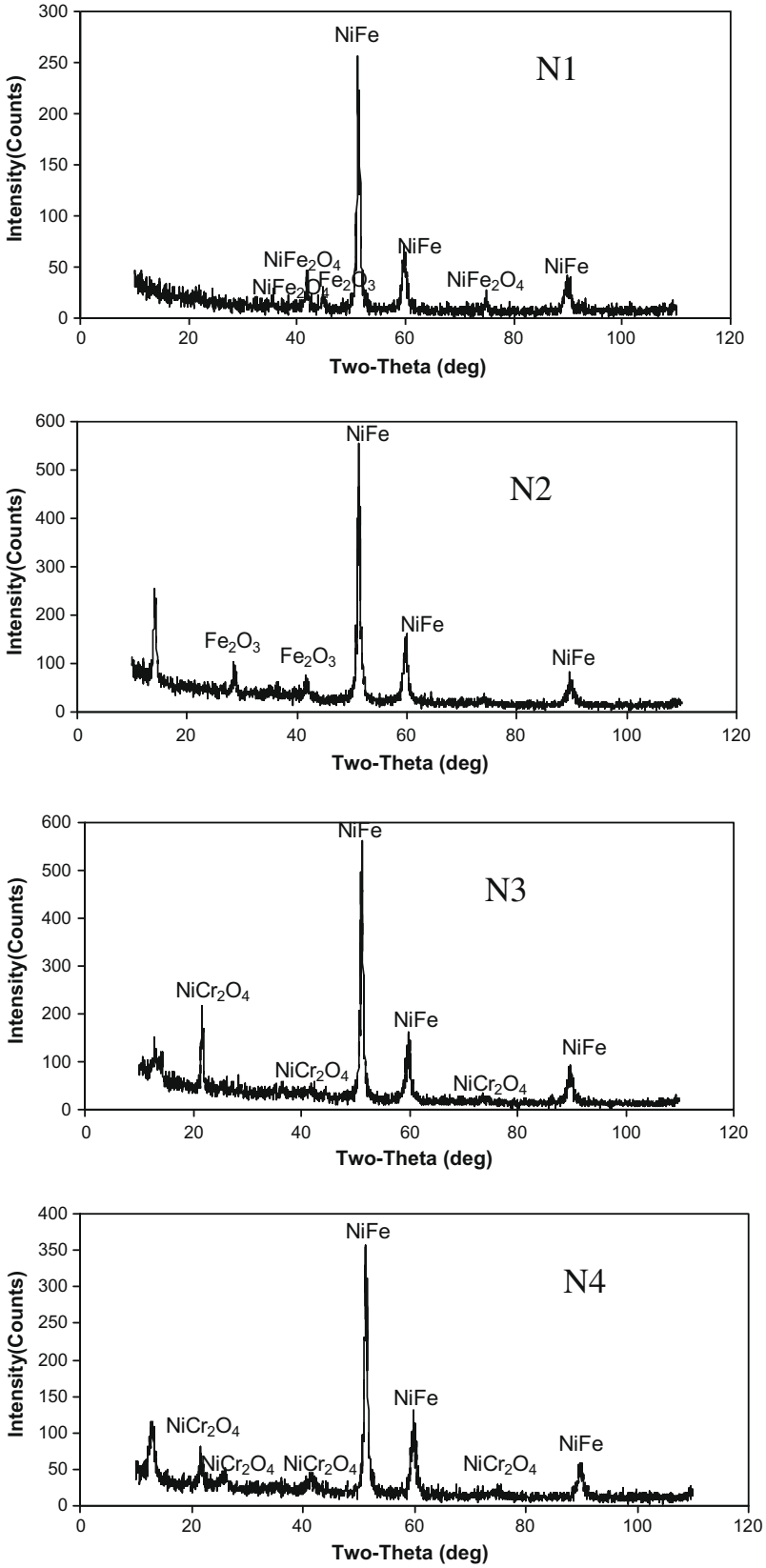

Fig. 6. XRD patterns of the films passivated at OCP at 300 °C in neutral solutions.

chemistries at 300 °C (Fig. 3). A strong magnesium peak indicated incorporation of magnesium during passivation. Calcium was also detected, especially when it coexisted with magnesium. The data summarized in Fig. 4 suggested that: (1) lead contamination reduced the chromium content and significantly increased the iron and nickel content in the passive film; (2) magnesium addition promoted ingress of calcium and reduced lead incorporation into the passive film. It is well known that chromium plays a key role

in the passivity of stainless steel [12]. The reduced chromium content will reduce the stability of the passive film. The detrimental effect of lead on the passivity will decline with decreasing lead concentration in the passive film [12].

According to Sato and Cohen [24], at the initial stage of passivation, a gel-like film that contains a large amount of M–OH and M–OH_2 bonds forms on the metal surface. Then the dehydration or aging of amorphous hydrates and/or hydroxides eventually brings about the formation of crystalline oxide film. It is well known the stability rank of bonds existing in passive film is M–O > M–OH > M–OH_2 [25–30]. Since the M–O bond is less reactive than M–OH and M–OH_2 bonds, the oxide film will be more protective than those containing a large proportion of hydroxides and/or hydrates. As revealed by previous studies, lead incorporation will hinder the dehydration process during passivation, resulting in the formation of passive film containing more less-stable M–OH/M–OH_2 bonds [11,12]. This also is well illustrated by the O_{1s} peak analysis shown in Fig. 5a and b. Comparing the data in Fig. 5b and c, we can see that magnesium addition reduces this kind of detrimental effect induced by the lead impurities. In passive film formed in the lead containing chemistry with the magnesium addition, the M–OH_2 bonds were undetectable, although the ratio of M–OH/M–O bonds did not change remarkably. Prior experimental evidence indicated a strong relationship between the rupture ductility and proportion of hydroxides/hydrates in passive film [12]. The passive films with high M–OH/M–OH_2 bonds had lower film rupture ductility. The lower film rupture ductility led to higher rupture frequency at crack tips when subjected to tensile load, hence a higher SCC susceptibility [12].

3.4. XRD analysis

In the Fe–Ni–Cr alloy system, the dehydration reaction may produce complex oxides with spinel structure [11,21].

$$(Ni,Fe)(OH)_2 + 2(Cr,Fe)(OH)_3 \rightarrow (Ni,Fe)(Cr,Fe)_2O_4 + 4H_2O \quad (2)$$

The spinel oxides are highly stable and so the formation of spinel oxides will improve the protective function of a passive film [31,32].

The hydrates and hydroxides are essentially amorphous and so cannot be detected using XRD techniques. The GIXRD patterns in Fig. 6a shows that spinel oxides were present in the passive film formed in lead-free chemistry (N1). In the passive film formed in the lead-contaminated chemistry (N2), the spinel oxides were undetectable (Fig. 6b). This confirmed that the incorporation of lead impurities into passive film hindered the dehydration and formation of spinel oxides during passivation [11,33]. Lead incorporation into the passive film may have led to formation of Pb-doped hydroxides (Eq. (3a)) [11,21].

$$Pb(OH)_2 + 2M(OH)_2 \rightarrow (OH)M{-}O{-}Pb{-}O{-}M(OH) + 2H_2O \quad (3a)$$

where M = (Fe, Ni), or (Eq. (3b)):

$$Pb(OH)_2 + 2M(OH)_3 \rightarrow (OH)_2M{-}O{-}Pb{-}O{-}M(OH)_2 + 2H_2O \quad (3b)$$

where M = (Cr, Fe). The hindered dehydration in passivation due to the lead incorporation implied that the Pb-doped hydroxides were more stable that the Pb-free ones.

When the magnesium species was added (N3 and N4), the spinel oxides became detectable again (Figs. 6c and d). This suggested that the presence of magnesium reduced the detrimental impacts on passivity. The XPS analysis showed that the presence of magnesium species in solution reduced the lead concentration in the passive film. A preliminary analysis indicated that the hydroxides were more defective than the crystalline oxides [21]. Therefore,

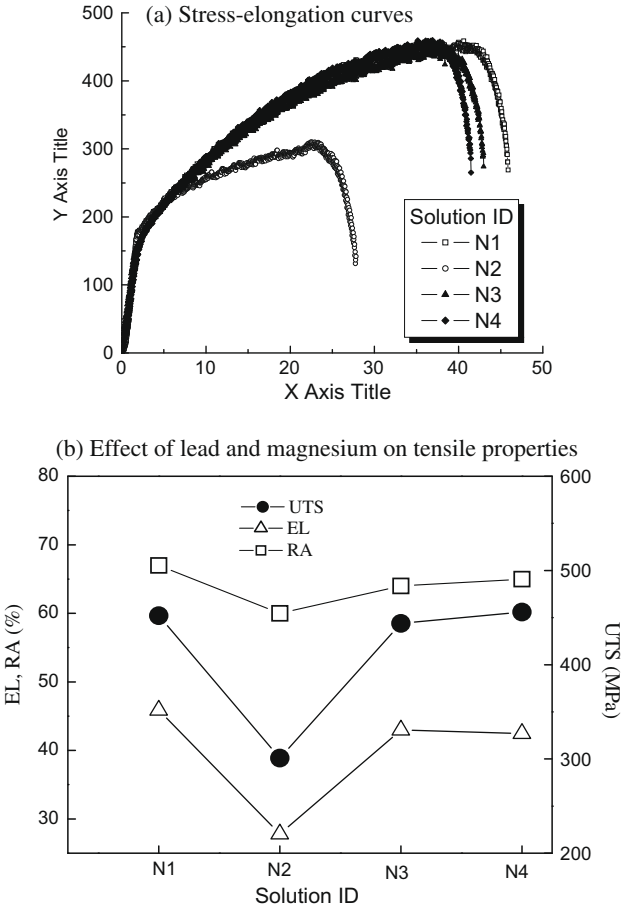

Fig. 7. Stress–elongation curves and mechanical properties measured by CERT tests.

the higher donor density in the passive film formed in the lead-contaminated chemistry (N2) probably was related to the hindered dehydration induced by lead impurities. The incorporation of magnesium decreased formation of Pb-doped hydroxides and promoted formation of the spinel oxides. In high temperature water, the predominant magnesium species was expected to be magnesium hydroxide [27]. However, the mechanism by which the magnesium blocked lead incorporation into the passive film is still unknown.

3.5. SCC behavior

The stress–strain curves in CERT tests conducted at 300 °C (Fig. 7a) showed that the presence of lead contamination promoted premature cracking and fracture of material, and that the addition of magnesium species compensated, at least partially, for the detrimental effect of lead contamination. The above statements were clearly demonstrated by the mechanical properties measured from the CERT tests summarized in Fig. 7b. Lead contamination reduced the ultimate tensile stress (UTS), the reduction of area (RA) and the elongation (EL), but this detrimental effect largely was compensated by the addition of magnesium ions. Similar to the passive current densities measured by potentiodynamic experiments (Fig. 1), the beneficial effect seemed to saturate gradually with increasing concentration of the magnesium species.

The above observations were supported by the fracture surface analysis (Fig. 8). The fracture surface in the lead-free solution (N1) consisted of dimple tearing fracture (Fig. 8a) indicating that the fracture was mainly ductile in nature. When the fracture occurred

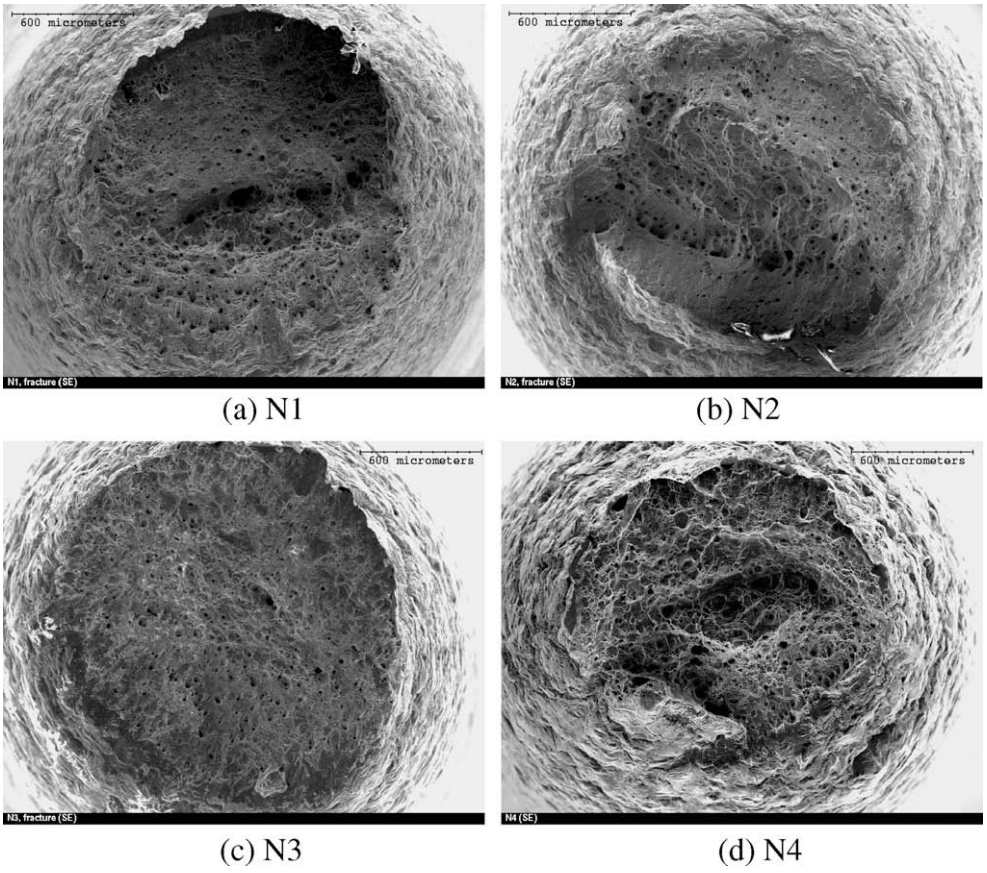

Fig. 8. SEM photographs of fracture surface.

in the lead-contaminated solution (N2), brittle fracture (cleavage-like) features were found (Fig. 8b) and some small cracks were detected on the side surface of the tensile specimen. The ratio of ductile to brittle area measured on the fracture surfaces obtained in the lead-free (N1) and the lead-contaminated solution (N1 vs. N2) were 3.53 and 0.56, respectively. These values indicated clearly that lead reduced the ductile area at the fracture surface. Addition of 0.075 M magnesium into the lead-contaminated solution (N3) reduced the brittle fracture feature (Fig. 7c). The brittle fracture feature almost disappeared as substitution by magnesium increased to 0.15 M (Fig. 8d). The ratio of ductile to brittle area ratios measured on the fracture surfaces obtained in N3 and N4 solutions were 2.73 and 3.00, respectively.

Thus there is a direct correlation between the SCC susceptibility and passivity of material. Our previous study revealed that the SCC susceptibility of Alloy 800 increases with the decreased rupture ductility of passive film, and the passive films with lower rupture ductility contained more hydroxides [12]. The presence of lead contamination reduced the rupture ductility of passive film and enhanced the SCC susceptibility [12]. The present study showed that the addition of magnesium species reduced the detrimental effect of lead contamination on the SCC resistance of Alloy 800 and this was related to the improved stability of the passive films. The magnesium species suppressed the detrimental effect of lead contamination on stability of passive film by: (1) reducing the effect of lead on the dehydration during passivity; (2) promoting the formation of spinel oxides; and (3) giving rise to the formation of passive film less defective and hence more protective. Further studies are needed to understand the mechanisms of the synergistic effect between calcium, magnesium and lead contamination in the feed water on the passivity and SCC susceptibility.

4. Conclusions

(1) Lead contamination enhances SCC susceptibility of Alloy 800 in neutral crevice chemistries at 300 °C and degrades passive film stability significantly.
(2) Addition magnesium to the solution increases the stability of passive films of Alloy 800 in lead-containing neutral crevice solution at 300 °C, as indicated by higher pitting potential, lower passive current density, smaller passive films having lower donor density, less hydroxides and more spinel oxides.
(3) Magnesium addition improves the SCC resistance of Alloy 800 in the lead-contaminated chemistries. The preliminary evidence suggests that the presence of magnesium affects SCC susceptibility in Pb-contaminated chemistries by altering passivation behavior of the material.

References

[1] R.W. Staehle, J.A. Gorman, Corrosion 59 (2003) 931–993. Part 2. Corrosion 6 (2004) 931–993. Part 3 Corrosion 59 (2003) 931–993.
[2] R.W. Staehle, Assessment of and proposal for a mechanistic interpretation of the SCC of high nickel alloys in lead containing environments, in: Proceedings of The 11th International Conference on Environmental Degradation of Materials In Nuclear Power System-water Reactors, vol.1, 2003.
[3] R.W. Staehle, Clues and issues in the SCC of high nickel alloys associated with dissolved lead, in: Proceedings of the 12th International Conference on Environmental Degradation of Materials in Nuclear Power System-water Reactors, 2005, pp. 1163.
[4] S.S. Hwang, H.P. Kim, D.H. Lee, U.C. Kim, J.S. Kim, Journal of Nuclear Materials 275 (1999) 28.
[5] D.G. Briceno, M.L. Castano, M.S. Garcia, Nuclear Engineering and Design 165 (1996) 161.
[6] S.S. Hwang, K.M. Kim, U.C. Kim, Stress corrosion cracking aspects of nuclear steam generator tubing materials in the water containing lead at high temperature, in: Proceedings of the 8th International Conference on

Environmental Degradation of Materials in Nuclear Power System-water Reactors, 1997.
[7] F. Cattant, M. Dupin., B. Sala, A. Gelpi, Analyses of deposits and underlying surfaces on the secondary side of pulled out tubes from a French plant, Contribution of materials investigation to the resolution of problems encountered in pressurized water reactors, in: Proceedings of the International Symposium, French Nuclear Society, Fontevraud III, 1994, p. 469.
[8] D.L. Harrod, R.E. Gold, R.J. Jacko, Journal of Material 53 (2001) 14.
[9] Y.C. Lu, Comparative studies on the localized corrosion susceptibility of Alloy 690 and Alloy800 under stimulated steam generator conditions, in: Proceedings of the 11th International Conference on Environmental Degradation of Materials in Nuclear Power System-water Reactors, Stevenson, Washington, 2003.
[10] S.S. Hwang, J.S. Kim, Corrosion 58 (2002) 392.
[11] B.T. Lu, J.L. Luo, Y.C. Lu, Journal of the Electrochemical Society 154 (2007) C379.
[12] B.T. Lu, J.L. Luo, Y.C. Lu, Electrochimica Acta 53 (2008) 4122.
[13] R.W. Bosch, W.F. Bogaerts, J.H. Zheng, Corrosion 59 (2003) 162.
[14] R. Memming, Philips Research Reports 19 (1964) 323.
[15] Y.C Lu, Effect of lead contamination on steam generator tube degradation, in: Proceedings of the 12th International Conference on Environmental Degradation of Materials in Nuclear Power System-water Reactors, 2005.
[16] S. Ahn, V.S. Rao, H.S. Kwon, U.C. Kim, Corrosion Science 48 (2006) 1137.
[17] CRC Handbook of Chemistry and Physics, Permittivity of Inorganic Solids, eighty-seventh ed., 2006–2007.
[18] S.R. Morrison, Electrochemistry at Semiconductor and Oxidized Metal Electrodes, Plenum Press, New York, 1980.
[19] A.M.P. Simoes, M.G.S. Ferreira, B. Rondot, M.C. Belo, Journal of Electrochemical Society 137 (1990) 82.
[20] D.D. Macdonald, Pure and Applied Chemistry 71 (1999) 951.
[21] B.T. Lu, B. Peng, J.L. Luo, Y.C. Lu, Passivity of nuclear steam generator tube alloy in lead-contaminated crevice chemistries with different pH, in: Proceedings of 13th International Conference on Environmental Degradation of Metals in Nuclear Power Systems, Paper No. 172, Whistler, BC, Canada, August 19-23, Canadian Nuclear Society, 2007.
[22] D. Costa, T. Tahala, P. Marcus, M Le calver, A. Gelpi, Interaction of lead with Nickel-base alloys 600 and 690, in: Proceedings of the 7th International Symposium on Environmental Degradation of Materials in Nuclear Power Systems-Water Reactors, 1995, pp. 199.
[23] S.S. Hwang, U.C. Kim, Y.S. Park, Journal of Nuclear Materials 246 (1997) 77.
[24] N. Sato, M. Cohen, Journal of Electrochemical Society 111 (1964) 512.
[25] B. Beverskog, I. Puigdomenech, Corrosion Science 38 (1996) 2121.
[26] B. Beverskog, I. Puigdomenech, Corrosion Science 39 (1997) 43.
[27] B. Beverskog, I. Puigdomenech, Corrosion Science 39 (1997) 969.
[28] M. Pourbaix, Atlas of Electrochemical Equilibrium, Pergamon Press, London, 1966.
[29] G. Okamoto, Corrosion Science 13 (1973) 471.
[30] W.P. Yang, D. Costa, P. Marcus, Journal of Electrochemical Society 141 (1995) 111.
[31] D. Cubicciotti, Journal of Nuclear Materials 201 (1993) 176.
[32] B. Beverskog, I. Puigdomenech, Corrosion 55 (1999) 1077.
[33] B. Peng, B.T. Lu, J.L. Luo, Y.C. Lu, Journal of Nuclear Materials 318 (2008) 333.